Science
AAAS

Aligned Multiwalled Carbon Nanotube Membranes
Bruce J. Hinds, *et al.*
Science **303**, 62 (2004);
DOI: 10.1126/science.1092048

These results can be improved by better modeling of the Galaxy and better understanding of the effects of various elements on the origin and evolution of life. For example, the abundances of radioactive species such as ^{26}Al play an important role in planet heating. However, to first order the overall metallicity is a good gauge of the abundances of other elements; the abundance (relative to solar) of most elemental species usually falls within a factor of two of the iron abundance (relative to solar) in nearby stars with a wide range of metallicity. Other factors that may play an important role should be visited in future studies. These include the frequency of grazing impacts with molecular clouds, the circularity of stellar orbits and their proximity to the corotation circle, and the effect of starbursts and an active Galactic nucleus in the early history of the most central regions of the Milky Way (*17*). If these additional constraints are used to further constrain the GHZ, it will encompass fewer stars, and the 10% quoted here will be recognized as an upper limit to the number of stars in the GHZ.

References and Notes

1. W. H. Tucker, in *Life in the Universe*, J. Billingham, Ed. (Massachusetts Institute of Technology Press, Cambridge, MA, 1981), pp. 287–296.
2. V. Trimble, *Origin Life Evol. Biosph.* **27**, 3 (1997).
3. G. Gonzalez, D. Brownlee, P. D. Ward, *Sci. Am.* **285**, 52 (October 2001).
4. G. Gonzalez, D. Brownlee, P. Ward, *Icarus* **152**, 185 (2001).
5. J. F. Kasting, D. P. Whitmire, R. T. Reynolds, *Icarus* **101**, 108 (1993).
6. Y. Fenner, B. K. Gibson, *Publ. Astron. Soc. Aust.* **20** 189 (2003).
7. C. H. Lineweaver, *Icarus* **151**, 307 (2001).
8. N. C. Santos, G. Israelian, M. Mayor, R. Rebolo, S. Udry, *Astron. Astrophys.* **398**, 363 (2003).
9. C. Laws *et al.*, *Astrophys. J.* **125**, 2664 (2003).
10. B. Carter, *Philos. Trans. R. Soc. London Ser. A* **310**, 347 (1983).
11. C. P. McKay, in *Circumstellar Habitable Zones*, L. R. Doyle, Ed. (Travis House, Menlo Park, CA, 1996), pp. 405–419.
12. M. Livio, *Astrophys. J.* **511**, 429 (1999).
13. D. H. Clark, W. H. McCrea, F. R. Stephenson, *Nature* **265**, 318 (1977).
14. J. Scalo, J. C. Wheeler, *Astrophys. J.* **566**, 723 (2002).
15. P. Kroupa, C. A. Tout, G. Gilmore, *Mon. Not. R. Ast. Soc.* **262**, 545 (1993).
16. H. Zinnecker, *Int. Astron. Union Symp.*, in press; preprint available online at http://arxiv.org/abs/astro-ph/0301080.
17. J. N. Clarke, *Icarus* **46**, 94 (1981).

18. The support of the Australian Research Council is gratefully acknowledged by all three authors. This collaboration was initiated at a meeting of ANITA, the Australian National Institute for Theoretical Astrophysics.

7 October 2003; accepted 20 November 2003

Aligned Multiwalled Carbon Nanotube Membranes

Bruce J. Hinds,[1,2]* Nitin Chopra,[1] Terry Rantell,[3] Rodney Andrews,[3] Vasilis Gavalas,[2] Leonidas G. Bachas[2]

An array of aligned carbon nanotubes (CNTs) was incorporated across a polymer film to form a well-ordered nanoporous membrane structure. This membrane structure was confirmed by electron microscopy, anisotropic electrical conductivity, gas flow, and ionic transport studies. The measured nitrogen permeance was consistent with the flux calculated by Knudsen diffusion through nanometer-scale tubes of the observed microstructure. Data on $Ru(NH_3)_6^{3+}$ transport across the membrane in aqueous solution also indicated transport through aligned CNT cores of the observed microstructure. The lengths of the nanotubes within the polymer film were reduced by selective electrochemical oxidation, allowing for tunable pore lengths. Oxidative trimming processes resulted in carboxylate end groups that were readily functionalized at the entrance to each CNT inner core. Membranes with CNT tips that were functionalized with biotin showed a reduction in $Ru(NH_3)_6^{3+}$ flux by a factor of 15 when bound with streptavidin, thereby demonstrating the ability to gate molecular transport through CNT cores for potential applications in chemical separations and sensing.

Advances in nanoporous membrane design with improvements in both chemical selectivity and high flux can directly benefit the fields of chemical separations, drug delivery, and wastewater remediation. Matching of pore size to that of the target molecules is critical to further advancement, because it will allow molecular sieving and forced interactions with chemically selective molecules bound to the pore. This is a particularly difficult challenge in the 1- to 10-nm size range. Numerous approaches are being investigated, including functionalized polymer affinity membranes (*1*), block copolymers (*2*), and mesoporous macromolecular architectures (*3*). Nanometer-scale control of pore geometry and demonstration of molecular separations have been achieved through the plating of nanoporous polycarbonate ion track-etch (*4*) and ordered alumina (*5*, *6*) membranes with initial pore dimensions of ~20 to 50 nm. A major challenge to improving the selectivities of pore-plated membranes is minimizing the variations in initial alumina pore diameters, because the resultant diameter is the difference between the plating thickness and the initial pore diameter. Thus, it is beneficial to start with a membrane structure that has an initial pore diameter near that of the target molecule diameter with small dispersion.

In principle, the inner cores of carbon nanotubes (CNTs) can enable fine control of pore dimension at the nanometer scale. During the CNT growth process, the nanotube size is set by the diameter of the catalyst particle (*7*, *8*), offering a practical route for pore diameter control through well-determined catalyst synthesis with nanometer-scale diameter dispersion (*9*, *10*). Transport through a single CNT with a 100-nm inner-core diameter, embedded across a polymer film, has been successfully demonstrated (*11*), but it is a substantial challenge to align large numbers (~10^{11} per cm^2) of CNTs with well-controlled nanometer-scale inner diameters across a robust membrane structure. Carbon has also been deposited into porous alumina structures by a template method, making an aligned CNT membrane (*12*). However, the inner diameters of these CNTs were ~50 nm, limiting their potential usefulness in molecular separation applications. There has also been a report of single-walled CNT alignment under extreme magnetic fields, but there was no microstructural characterization to show flux through the inner cores of the CNTs as opposed to flow across a dense matting of CNTs (*13*). The aligned growth of dense arrays of multiwalled CNTs has been demonstrated (*14*–*17*). Although the outer diameters had substantial variation (30 ± 10 nm), the hollow inner-core diameter was well controlled at 4.3 ± 2.3 nm, because more outer graphite walls were added with larger catalyst sizes (*14*). This inner-core diameter is in the size range of many proteins and other important biological macromolecules. The primary goal of our work was to form membrane structures that take advantage of the as-deposited alignment of multiwalled CNTs to form a well-controlled nanoporous membrane structure and to demonstrate molecular transport through the CNT cores.

Figure 1A shows a scanning electron microscope (SEM) micrograph of as-grown multiwalled CNTs, indicating the character-

[1]Department of Chemical and Materials Engineering, [2]Department of Chemistry, University of Kentucky, Lexington KY 40506, USA. [3]Center for Applied Energy Research, 2540 Research Park Drive, Lexington, KY 40511, USA.

*To whom correspondence should be addressed. E-mail: bjhinds@engr.uky.edu

istic high degree of vertical alignment. The ideal membrane structure will occur when the space between the CNTs is filled with a continuous polymer film and the normally closed ends of the CNTs are etched open (Fig. 1B). To accomplish this, we grew CNTs for 30 min (with an aligned CNT film thickness of 5 to 10 μm) on quartz substrate, in a chemical vapor deposition process that used a ferrocene-xylene-argon-hydrogen feed at 700°C (*14*). A 50 weight-percent solution of polystyrene (PS) and toluene was spin-coated over the surface (*18*). PS is known to have high wetability with CNTs, and the CNT array was readily impregnated with PS (*19*). Because of the high viscous drag within the CNT array, only excess polymer on top of the composite structure was removed during the spin-coating process. The film was dried in vacuum at 70°C for 4 days. Hydrofluoric acid was then used to remove the CNT-PS composite from the quartz substrate, to produce a freestanding composite film of 5- to 10-μm thickness. Figure 1C shows the cleaved edge of the freestanding membrane structure, with CNT alignment intact from top to bottom of the polymer film. A few cut CNTs with high curvature were artifacts of the cleaving and plasma oxidation process. A tortuosity of 1.10 (±0.05) was estimated from the CNT length divided by the film thickness, obtained from cross-sectional micrographs. We then removed a thin layer of excess polymer from the top surface and opened the CNT tips to form a membrane structure. This was accomplished with a H_2O plasma-enhanced oxidation process at 600 mtorr H_2O pressure and 2.5 W/cm^2 for 7 min, similar to conditions used to remove Fe nanocrystal catalyst particles from the tips of CNTs (*20*).

The overall processing scheme for the CNT membrane is shown in fig. S1. The plasma oxidation process etches PS faster than CNTs; thus, the CNT tips were 10 to 50 nm above the polymer surface. SEM analysis of this surface gave an estimated areal density of 6 (±3) × 10^{10} CNT tips per cm^2. Importantly, the plasma process left the tips of the CNTs functionalized with carboxylate groups that could be readily reacted with biomolecules, including a wide variety of selective receptors (*21–23*). Transmission electron microscopy (TEM) of dissolved membranes (figs. S2 and S3) demonstrated that ~70% of the CNT tips had been opened by the plasma oxidation process under our conditions. Substantial amounts of Fe catalyst were observed in the cores of the CNTs, but were reduced by 24 hours of HCl treatment. Electrical transport measurements were also consistent with the presence of highly conductive CNTs that span from top to bottom of the insulating polymer film. The conductivity from top to bottom of the membrane (Au film contacts) was 35.2 Ω^{-1}cm^{-1}, whereas a 4-point probe that measured sheet resistance gave an in-plane conductivity value two orders of magnitude less than that, at 0.32 Ω^{-1}cm^{-1}. Reduced in-plane conductivity would be expected, because neighboring CNTs only touched each other with the modest tortuosity seen in Fig. 1C.

Transport measurements of both gas (N_2) and aqueous ionic species [$Ru(NH_3)_6^{3+}$] were performed to determine transport through the inner cores of the CNTs. For room-temperature N_2 permeance measurements, CNT membranes were epoxy-sealed between macroporous, glass-fiber, disk filters and mounted in a gas-flow system equipped with a water manometer. The gas-flow volume was measured by a calibrated mass-flow meter with the exhaust line at atmospheric ambient pressure. Figure 2A indicates a permeance of 2.6 μmol/(m^2 s Pa), quite comparable to the permeance of nanometer-scale, porous alumina membrane structures (*24*). Using Knudsen diffusion, in which the gas-molecule mean free path is limited by pore radius, we can calculate the molar flux (N_a) as $N_a = \varepsilon D_k(P_1 - P_2)/RTLa$, where ε is the void fraction, $P_1 - P_2$ is the pressure difference, R is the universal gas constant, T is the absolute temperature, L is the pore length, a is tortuosity, and D_k is the Knudsen diffusion coefficient,

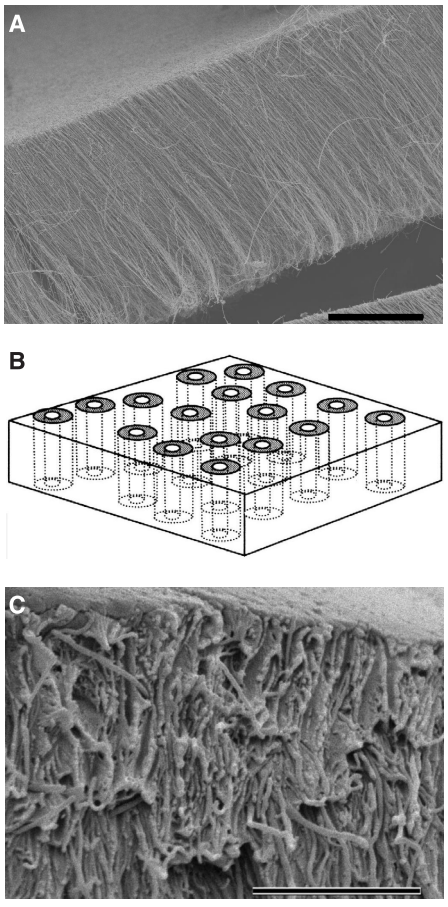

Fig. 1. (**A**) An as-grown, dense, multiwalled CNT array produced with an Fe-catalyzed chemical vapor deposition process (*18*). Scale bar, 50 μm. (**B**) Schematic of the target membrane structure. With a polymer embedded between the CNTs, a viable membrane structure can be readily produced, with the pore being the rigid inner-tube diameter of the CNT. (**C**) The cleaved edge of the CNT-PS membrane after exposure to H_2O plasma oxidation. The PS matrix is slightly removed to contrast the alignment of the CNTs across the membrane. Scale bar, 2.5 μm.

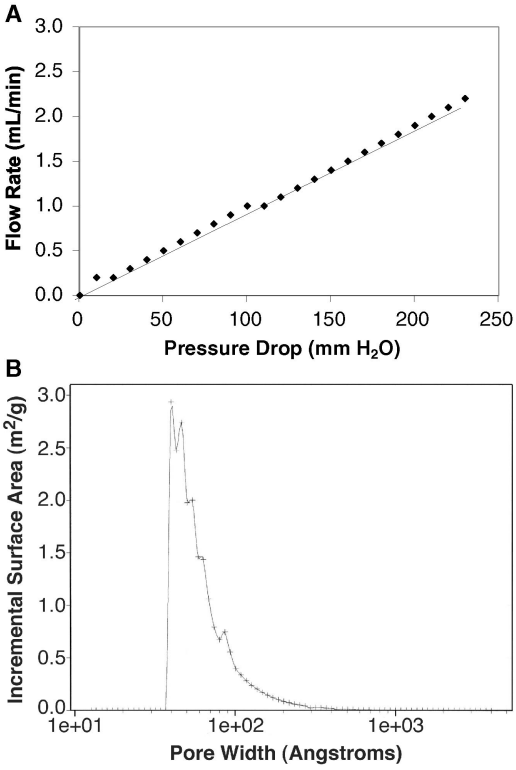

Fig. 2. (**A**) N_2 gas flow through the CNT membrane structure with a 3.1-cm^2 surface area and 5-μm thickness. The slope gives a permeance of 2.6 μmol/(m^2 s Pa). (**B**) N_2 Porosity data at 77 K, showing a pore distribution of 6 ± 2 nm, consistent with TEM observations of the CNT inner-core diameter.

which can be calculated as $D_k = 0.97r\,(T/M_a)^{1/2}$, where r is the mean pore radius and M_a is the molecular weight of the permeate molecule. Using Knudsen diffusion, an observed CNT areal density of 6 ($\pm$ 3) $\times$ 10^{10} per cm^2, mean pore diameter of 7.5 ($\pm$2.5) nm, diffusion length of 5 ($\pm$1) μm, and tortuosity of 1.10 ($\pm$0.05), we calculated a permeance of 2.4 ($\pm$1.9) μmol/(m^2 s Pa). This is consistent with the observed microstructure of open CNTs that pass across the PS film. A void fraction ε of 0.027 was calculated from the CNT areal density and the inner-core cross-sectional area. Figure 2B shows pore size distribution from N_2 desorption at 77 K. The pore size distribution matches that of the CNT inner-core diameter that was observed by TEM (*14*) and is consistent with the premise of an aligned CNT membrane structure. The porosimeter data on the aligned CNTs without embedded polymer (Fig. 1A) show a peak of characteristic CNT inner-core diameters (6 to 10 nm) (Fig. 2B) and a very broad tail of 20- to 100-nm pore sizes, which are associated with N_2 adsorption on the outer surfaces of CNTs in a densely aligned mesh. When CNTs were embedded within the polymer film, this tail feature did not appear in the porosimeter measurement, which is consistent with a polymer filling the space between the CNTs. Thus, the observed flow through the membrane was through the accessible inner cores of the CNTs. The observed pore volume from N_2 desorption experiment was 0.073 cm^3/g. This is consistent with the estimated pore volume of 0.028 ($\pm$0.013) cm^3/g, calculated from the CNT areal density (6 $\times$ 10^{10} per cm^2), the inner-core projected area (πr^2, where $2r$ = 7.5 nm), the tube length (5 μm), the tortuosity (1.10), and the PS density (1.05 g/cm^3).

The aligned CNT membrane structure also allowed the transport of $Ru(NH_3)_6^{3+}$ ions in aqueous solution. A 10-μm-thick membrane was epoxy-sealed to one end of a Pyrex tube, and 400 μL of a 0.01 M KCl solution was placed inside the Pyrex tube. The membrane was submerged in a 5 mM $(Ru(NH_3)_6Cl_3)$:0.01 M KCl reference solution, to establish a Ru concentration gradient. The inner solution was kept level with the outer reference solution to avoid any pressure-induced transport. The flux of Ru ions passing through the membrane into the inner solution was then determined by cyclic voltammetry. For the aligned CNT membrane after H_2O plasma oxidation, a $Ru(NH_3)_6^{3+}$ flux of 0.07 μmol cm^{-2} hour^{-1} was observed. Treatment of the membrane with HCl for 24 hours aided the ionic flux substantially, increasing it to 0.9 μmol cm^{-2} hour^{-1}, presumably by dissolving excess Fe not removed by the plasma process. This flux is comparable to that of ordered alumina membranes showing fluxes of a benzonitrile enantiomer of 0.3 μmol cm^{-2} hour^{-1} (*8*). The diffusion coefficient (D) of $Ru(NH_3)_6^{3+}$ through the membrane was found to be 2.2 ($\pm$0.9) $\times$ 10^{-6} cm^{-2} s^{-1} from the measured flux, with the areal density, pore diameter, thickness, and tortuosity given previously. This is near the bulk aqueous-solution diffusion for $Ru(NH_3)_6^{3+}$ of 7 $\times$ 10^{-6} cm^{-2} s^{-1} (*25*), indicating only modest interaction of the ion with the CNT tip and the core. We would expect negatively charged carboxylate functional groups at the tips to reduce the observed diffusion coefficient of a positively charged $Ru(NH_3)_6^{3+}$ ion. In a control experiment, membranes without H_2O plasma treatment did not show ionic transport. Therefore, diffusion through the solid polymer was not significant. Backlit optical microscopy after electrochemical characterization did not show any signs of micro-cracking.

Importantly, the open tips of the CNTs with carboxyl end groups were readily functionalized, which could form the basis for gatekeeper-controlled chemical separations or an ion-channel mimetic sensor. If a selective functional molecule were placed at the entrance of the CNT and coordinated with a bulky receptor, the CNT pore would be blocked and the ionic flow through the CNT core would be reduced. Ionic flow could be easily detected electrochemically and could provide the basis of a selective sensor system. For a demonstration, the well-established biotin/streptavidin analyte/receptor system was chosen. (+)-Biotinyl-3,6 dioxaoctanediamine (Pierce Biotechnology EZ-Link) was reacted with the carboxylate end groups of the CNT membrane with a carbodiimide-mediated reaction. This was subsequently coordinated with streptavidin. Figure 3 shows the flux of $Ru(NH_3)_6^{3+}$ ions for the as-prepared aligned CNT membrane after biotin functionalization and coordination with streptavidin. With the attachment of the biotin tether (2.2 nm long), the $Ru(NH_3)_6^{3+}$ flux was reduced by a factor of 5.5. Simple cross-sectional area reduction of the CNT inner core diameter (from 7.5 nm to 3.1 nm) would reduce ionic flux by a factor of 6.2; thus, this system shows promise for the use of dimensions of attached molecules to further control pore dimensions. The ionic flux was further reduced by a factor of 15 on streptavidin coordination with biotin. This ap-

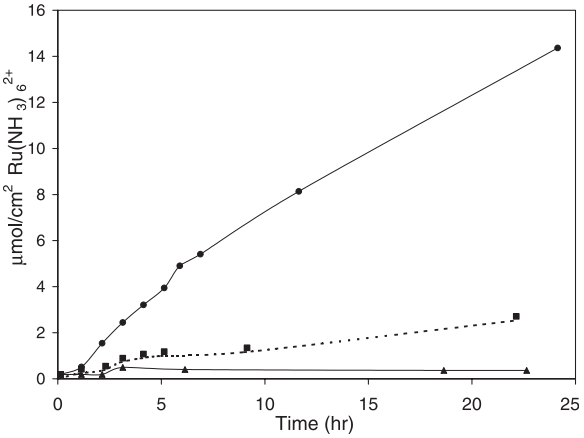

Fig. 3. $Ru(NH_3)_6^{3+}$ flux through a CNT membrane structure after HCl treatment (circles), after biotin functionalization (squares), and after streptavidan coordination (triangles). Source solution was 5 mmol $Ru(NH_3)_6^{3+}$, analyte volume was 0.4 ml, and membrane area was 0.028 cm^2. $Ru^{2+/3+}$ concentration was analyzed by electrochemical oxidation peak height at $-$0.25 V versus Ag-AgCl as compared to a reference solution.

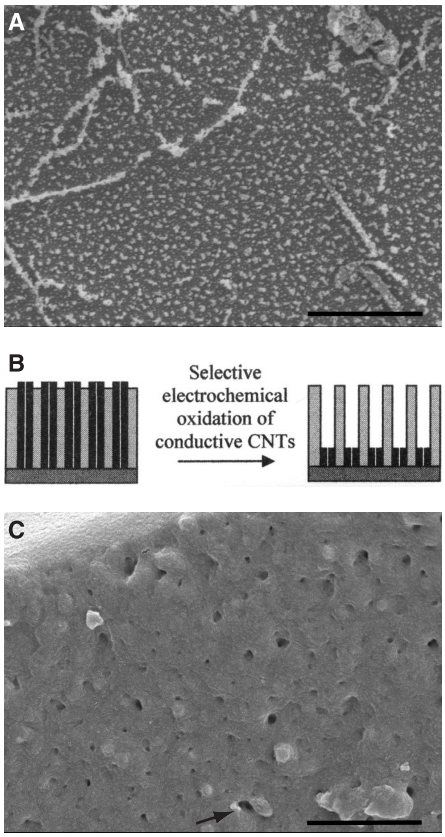

Fig. 4. (**A**) The surface of the CNT-PS membrane after H_2O plasma treatment. CNTs are above the film surface because of the faster etching rate of the polymer. (**B**) Schematic for selective oxidation of conductive CNTs only. (**C**) Resultant film surface after electrochemical oxidation of CNTs at 1.7 V versus Ag-AgCl, below the surface of the contiguous polymer film. The arrow indicates a smaller surface pore nested inside a larger surface pore. Scale bar, 2.5 μm.

proach of functionalizing the entrance to each CNT core can be generalized to a variety of biological affinity pairs to block ionic flow through the CNT core when the analyte is present.

Electrochemistry can also be used to tailor the aligned CNT membrane structure. Practical considerations of membrane strength and aligned CNT growth require that the membrane be at least 5 μm thick. However, for large molecular separations based on gate-keeper selectivity, a short path length is desired, because it increases the diffusion flux. One possible route to trim the CNT length is to anodically oxidize the CNTs at +1.7 V versus an Ag-AgCl reference electrode (*26*). Because the PS polymer is an insulator, the conductive CNTs are selectively etched within the polymer matrix. Thus, one can adjust pore length while maintaining the mechanical integrity of the thicker PS matrix. Figure 4A shows the surface of membrane films after H_2O plasma oxidation. The tips of the CNTs are extending above the surface because of the faster etching rate of PS by plasma treatment. Each bright area in Fig. 4A corresponds to the tips of multiple (*2*–*7*) CNTs clustered together, resulting in outer diameters of ~50 nm that are consistent with TEM observations. An areal density of 6 (± 3) $\times 10^{10}$ per cm^2 can be estimated from this micrograph. Figure 4B shows a schematic cross section illustration of how CNTs could be selectively oxidized electrochemically inside an insulating PS matrix. Figure 4C shows the surface after selective electrochemical oxidation. The size of the pores on the PS surface should be at least that of the 40-nm outer CNT diameter (Fig. 4B). Because the tips of the CNTs tend to group together and there is the possibility of localized PS oxidation next to the CNTs, the resulting PS surface pores were often greater than 100 nm. Figure 4C (arrow) shows an example of a smaller PS surface pore inside a larger PS surface pore, which is consistent with clustering of CNT tips at the surface.

Selective reduction of the length of CNTs within the PS matrix can be a valuable tool for tuning membranes to give a required flux while keeping carboxylate functionalization at the tips of CNTs. These carboxylate end groups can then be readily functionalized at the entrance of each CNT inner core to selectively gate molecular transport through the ordered nanoporous membrane for separation and sensing applications.

References and Notes

1. E. Klein, *J. Membr. Sci.* **179**, 1 (2000).
2. T. Thurn-Albrecht *et al.*, *Adv. Mater.* **12**, 787 (2000).
3. J. T. Asefa, M. J. MacLachlan, N. Coombs, G. A. Ozin, *Nature* **402**, 867 (1999).
4. K. B. Jirage, J. C. Hulteen, C. R. Martin, *Science* **278**, 655 (1997).
5. E. D. Steinle *et al.*, *Anal. Chem.* **74**, 2416 (2002).
6. S. B. Lee *et al.*, *Science* **296**, 2198 (2002).
7. H. Kanzow, C. Lenski, A. Ding, *Phys. Rev. B* **6312**, 5402 (2001).
8. H. Ago, T. Komatsu, S. Ohshima, Y. Kuriki, M. Yumura, *Appl. Phys. Lett.* **77**, 79 (2000).
9. L. Sun, R. M. Crooks, *J. Am. Chem. Soc.* **122**, 12340 (2000).
10. S. A. Miller, C. R. Martin, *J. Electroanal. Chem.* **522**, 66 (2002).
11. H. Ago, T. Komatsu, S. Ohshima, Y. Kuriki, M. Yumura, *Appl. Phys. Lett.* **77**, 79 (2000).
12. C. L. Cheung, A. Kurtz, H. Park, C. Lieber, *J. Phys. Chem. B* **106**, 2429 (2002).
13. M. J. Casavant, D. A. Walters, J. J. Schmidt, R. E. Smalley, *J. Appl. Phys.* **93**, 2153 (2003).
14. R. Andrews *et al.*, *Chem. Phys. Lett.* **303**, 467 (1999).
15. Z. F. Ren *et al.*, *Science* **282**, 1105 (1998).
16. V. I. Merkulov *et al.*, *Appl. Phys. Lett.* **80**, 4816 (2002).
17. Z. J. Zhang, B. Q. Wei, G. Ramanath, P. M. Ajayan, *Appl. Phys. Lett.* **77**, 3764 (2000).
18. Materials and methods are available as supporting material on *Science* Online.
19. D. Qian, E. C. Dickey, R. Andrews, T. Rantell, *Appl. Phys. Lett.* **76**, 2868 (2000).
20. S. M. Huang, L. M. Dai, *J. Phys. Chem. B* **106**, 3543 (2002).
21. M. A. Hamon, H. Hui, P. Bhowmik, H. M. E. Itkis, R. C. Haddon, *Appl. Phys. A* **74**, 333 (2002).
22. C. V. Nguyen *et al.*, *Nano Letters* **2**, 1079 (2002).
23. J. L. Bahr, J. M. Tour, *Chem. Mater.* **13**, 3823 (2001).
24. X. Pages, V. Rouessac, D. Cot, G. Nabias, J. Durand, *Sep. Purif. Tech.* **25**, 399 (2001).
25. D. O. Wipf, E. W. Kristensen, M. R. Deakin, R. M. Wightman, *Anal. Chem.* **60**, 306 (1988).
26. T. Ito, L. Sun, R. M. Crooks, *Electrochem. Solid State Lett.* **6**, C4 (2003).

27. We thank W. Shafer for porosity measurements, D. Qian for the growth of aligned CNTs, A. Jeromczyk for aid with electrochemical measurements, and A. Dozier for aid with TEM characterization. Supported by a Kentucky Science and Engineering Foundation seed grant, by the NSF Materials Research Science and Engineering Center's Advanced Carbon Materials Center (grant no. DMR-9809686), and by NASA and Air Force Research Laboratory (agreement no. F49620-02-1-0225).

Supporting Online Material

www.sciencemag.org/cgi/content/full/1092048/DC1
Materials and Methods
Figs. S1 to S3

9 September 2003; accepted 17 November 2003
Published online 27 November 2003;
10.1126/science.1092048
Include this information when citing this paper.

Supramolecular Self-Assembly of Macroscopic Tubes

Deyue Yan,* Yongfeng Zhou, Jian Hou

The macroscopic molecular self-assembly of an amphiphilic hyperbranched copolymer in acetone generated multiwalled tubes millimeters in diameter and centimeters in length. The thickness of the tube walls approaches 400 nanometers, and the walls have an inhomogeneous lamella structure that alternates between ordered hydrophilic domains and amorphous, partly irregular hydrophilic domains.

Molecular self-assembly of organic molecules has generated a wide variety of objects with nanoscale or micrometer-scale morphologies, including micelles (*1, 2*), vesicles (*3*–*5*), ribbons (*6*), films (*7*), fibers (*8*–*10*), and tubules (*11*–*13*). These reported self-assembled objects were predominantly generated from organic molecules with well-defined size and structure. To date, little attention has been paid to molecular self-assembly originating from ill-defined macromolecules such as hyperbranched copolymers. We now report the molecular self-assembly of tubes with macroscopic dimensions.

When an amphiphilic hyperbranched multi-arm copolymer was added to a selective solvent, macroscopic tubes with centimeter-scale length and millimeter-scale diameter appeared. The hyperbranched multi-arm copolymer (HBPO-star-PEO; Fig. 1) is an amphiphilic macromolecule with a hydrophobic hyperbranched poly(3-ethyl-3-oxetanemethanol) core (HBPO) and many hydrophilic poly(ethylene glycol) arms (PEO). The molecular weight of the core precursor, as characterized by size exclusion chromatography (SEC), is 8560 (10,500 by the vapor-pressure osmometer); the polydispersity index is 1.5, and the degree of branching measured by ^{13}C nuclear magnetic resonance (NMR) is 0.45 (*14*). When 3 g of the dried viscous jelly-like HBPO-star-PEO was directly added to 30 ml of acetone under stirring conditions at room temperature, macroscopic tube self-assembly was observed. [Details of the preparation, characterization, and self-assembly of HBPO-star-PEO are given in (*14*).] A photograph of the resulting self-assembly objects (Fig. 2) reveals transparent tubes that can be seen with the naked eye. The diameter of the tubes approaches 1 mm, and the average length of the tubes is about 1.8 cm (except those broken by vigorous stirring). The length of the longest tubes formed in other batches approaches 7.5 cm, and the diameter of the largest tube is 1.5 mm (*15*). In addition, there are a number of imperfect tubes in Fig. 2. For instance, object **a** is a fractured tube that mediates between a tube and a film, and object **b** is a twin tube made of a curly film.

The macroscopic morphology of the tubes was also observed by optical microscopy. A pentawalled tube with the coaxial cylindrical

College of Chemistry and Chemical Engineering, Shanghai Jiao Tong University, 800 Dongchuan Road, Shanghai, 200240, People's Republic of China.

*To whom correspondence should be addressed. E-mail: dyyan@sjtu.edu.cn